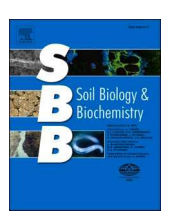
ELSEVIER

Contents lists available at ScienceDirect

# Soil Biology and Biochemistry

journal homepage: www.elsevier.com/locate/soilbio



# Where and why do particulate organic matter (POM) and mineral-associated organic matter (MAOM) differ among diverse soils?

Wenjuan Yu<sup>a,\*</sup>, Wenjuan Huang<sup>a</sup>, Samantha R. Weintraub-Leff<sup>b</sup>, Steven J. Hall<sup>a</sup>

#### ARTICLE INFO

Keywords:
Soil organic matter
Physical fraction
Stable isotope
Decomposition
Soil geochemistry
National ecological observatory network
(NEON)

#### ABSTRACT

Soil organic matter (SOM) has often been separated into operational physical fractions, such as particulate organic matter (POM) and mineral-associated organic matter (MAOM), to improve our understanding of SOM persistence. While it is generally assumed that POM and MAOM have distinct biogeochemical characteristics, it remains unresolved where and why POM and MAOM differ in their composition and relationships to total SOM decomposition among heterogenous soils. We analyzed elemental, isotopic, and chemical composition, including diffuse reflectance infrared Fourier transform (DRIFT) spectra, of POM and MAOM in 156 soil samples collected from 20 National Ecological Observatory Network (NEON) sites spanning diverse ecosystems (tundra to tropics) across North America. We used a classic size separation method for POM (53–2000  $\mu m$ ) and MAOM ( $<53~\mu m$ ) following chemical dispersion. Values of C/N,  $\delta^{13}$ C, and DRIFT spectra for C-H (aliphatic)/C=O were correlated and often similar in POM and MAOM fractions across diverse soils; DRIFT spectra for C=C (aromatic)/C=O were often similar but uncorrelated between fractions. A prevalent hypothesis holds that MAOM is dominated by microbial-derived OM, yet our findings suggest that plant-derived OM can also contribute substantially to MAOM, especially in wet forests receiving >1200 mm annual precipitation (with MAOM C/N > 15). Multiple statistical analyses showed that C quantity and chemical composition of MAOM could as effectively predict soil C decomposition during an 18-month incubation as measures of POM. Thus, POM and MAOM both likely contributed significantly to decomposition over timescales of months, possibly because characteristics of POM and MAOM were often related and/or a large pool size of MAOM could compensate for its lower decomposition rate relative to POM. Further, we found that soil geochemical composition (such as silt and clay, calcium, oxalate-extractable iron and aluminum), along with climate and ecosystem type, could partly predict differences in quantity and composition between POM and MAOM. Overall, relative coupling vs. decoupling between POM and MAOM among soils was predictable based on geochemistry, and these similarities/differences provide insight into variation in the plant-derived sources of MAOM across diverse ecosystems. The importance of MAOM to short-term soil C decomposition has probably been underappreciated.

#### 1. Introduction

Soil organic matter (SOM) has often been separated experimentally into different physical fractions, under the hypothesis that physical fractions are related to theoretical pools with differing decomposition rates because of differences in protection mechanisms and biogeochemical characteristics (Christensen, 1996; Smith et al., 2002). Physical separation of SOM into operational measures of particulate organic matter (POM) and mineral-associated organic matter (MAOM) by size and/or density, following dispersion of aggregates, is a classic approach

that remains popular in the research community, and it has led to important insights about SOM distribution and responses to environmental change (Cambardella and Elliott, 1992; Song et al., 2012; Follett et al., 2015; Cotrufo et al., 2019; Witzgall et al., 2021; Heckman et al., 2022). POM and MAOM are typically hypothesized to have distinct biogeochemical properties and turnover rates as a consequence of their presumed differences in sources (e.g., plant vs. microbial residues) and degrees of physicochemical protection (Lavallee et al., 2020). However, both POM and MAOM fractions are also known to contain mixtures of faster- and slower-cycling C pools with likely contributions from both

E-mail address: wjyu@iastate.edu (W. Yu).

<sup>&</sup>lt;sup>a</sup> Department of Ecology, Evolution, and Organismal Biology, Iowa State University, Ames, IA, USA

<sup>&</sup>lt;sup>b</sup> National Ecological Observatory Network, Battelle, Boulder, CO, USA

<sup>\*</sup> Corresponding author.

plant and microbial detritus (von Lützow et al., 2007; Torn et al., 2013; Hall et al., 2015; Poeplau et al., 2018; Angst et al., 2021). These conflicting findings point to an unresolved question: how different are POM and MAOM in their biogeochemical characteristics and their relationships to soil C decomposition across diverse environments, and what factors influence the differences between these operational fractions? Further clarifying our interpretation of these commonly measured

fractions could improve mechanistic understanding of SOM dynamics and help to clarify the sources and persistence mechanisms of SOM within and among ecosystems.

It is still unclear whether POM and MAOM could similarly predict soil organic carbon (SOC) decomposition across diverse soils. On one hand, POM and MAOM are generally considered to have decoupled turnover rate, source and composition, POM is often assumed and

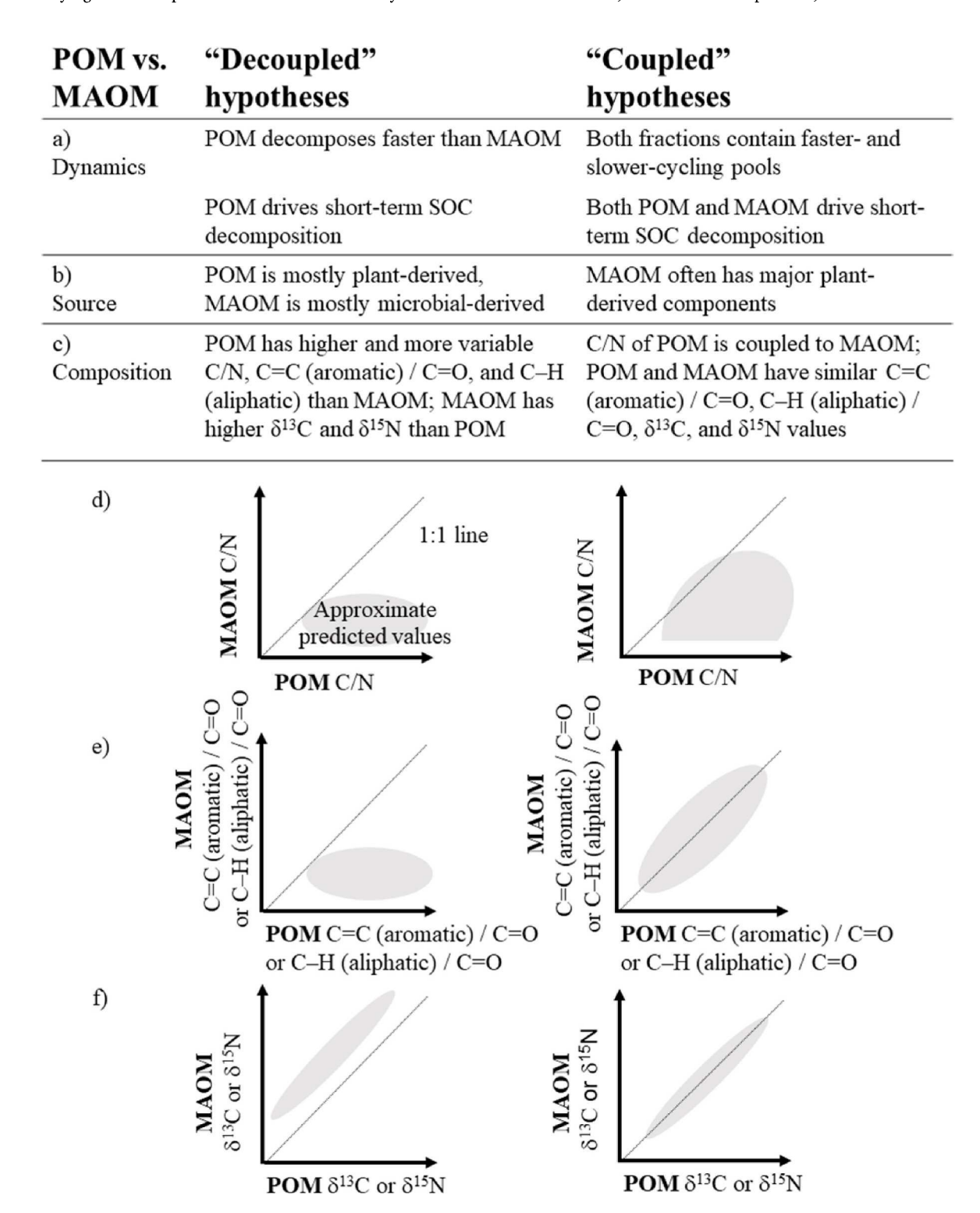


Fig. 1. Conceptual hypotheses of differences in dynamics, source, and composition between POM and MAOM. Under "Decoupled" hypotheses, POM dominates short-term SOC decomposition and POM and MAOM have generally decoupled source and composition; under "Coupled" hypotheses, both POM and MAOM drive short-term SOC decomposition and POM and MAOM often have coupled source and composition. Shaded areas: approximate predicted values based on previous work. Dotted line: the 1:1 relationship for a given variable.

demonstrated to decompose more rapidly than MAOM (Parton et al., 1987; Feng et al., 2016), and POM generally has shorter residence times (years-decades) than MAOM (decades-centuries) based on <sup>14</sup>C analysis (Kleber et al., 2015). Thus, POM may dominate heterotrophic respiration (Elliott, 1986; Arevalo et al., 2012) and may be a good predictor of short-term SOC decomposition, measured as soil respiration (Alvarez and Alvarez, 2000). We summarize these ideas in Fig. 1a as a hypothesized "decoupling" of dynamics of POM and MAOM. On the other hand, both POM and MAOM contain faster- and slower-cycling components (Torn et al., 2013; Paul, 2016), and a relatively fast-cycling MAOM component with annual to decadal turnover times appears to be present in many soils (von Lützow et al., 2007; Torn et al., 2013; Hall et al., 2015; Keiluweit et al., 2015; Giannetta et al., 2019). MAOM might also be a major contributor to SOC decomposition, especially in cases where a large pool size of MAOM compensates for its lower decomposition rate relative to POM (Christensen 1987). We summarize these ideas in Fig. 1a as a hypothesized "coupling" of dynamics of POM and MAOM.

In addition to their potential differences in turnover (Fig. 1a), POM and MAOM are also expected to differ in their sources and biochemical composition (Fig. 1b and c, Decoupled hypotheses; Lavallee et al., 2020). POM is thought to be largely made up of partially decomposed plant residues (Baldock and Skjemstad, 2000), while microbial necromass and metabolites have been proposed as a major source for C in MAOM based on the Microbial Efficiency-Matrix Stabilization (MEMS) hypothesis (Cotrufo et al., 2013; Liang et al., 2017). According to this hypothesis (Fig. 1b Decoupled), high-quality litters would be efficiently converted to microbial biomass and necromass that form organo-mineral associations and accumulate in MAOM (Cotrufo et al., 2013). A growing body of evidence supports this hypothesis by showing that microbial processing of higher-quality substrates resulted in more MAOM C than low-quality ones (Cyle et al., 2016; Lavallee et al., 2018) and MAOM stored much more microbial necromass than POM (Griepentrog et al., 2014; Angst et al., 2019).

Based on this hypothesis (Fig. 1b Decoupled), we infer that POM should have generally higher and more variable C/N ratios than MAOM and their C/N ratios should be relatively decoupled (Fig. 1c and d Decoupled hypothesis), as the  $\ensuremath{\text{C/N}}$  of POM and MAOM should largely correspond to the C/N of plant litter and microbial necromass, respectively. Plant litters vary substantially in their C/N ratio (e.g., 40-120 across a subset of National Ecological Observatory Network (NEON) sites; Hall et al., 2020) while soil microbes have a lower and more constrained C/N ratio (3-15; Strickland and Rousk, 2010). Lavallee et al. (2020) proposed that POM generally has C/N ratios between 10 and 40 while MAOM has C/N ratios between 8 and 13. By this logic, we expect differences between MAOM and POM in their C functional groups, as measured by diffuse reflectance infrared Fourier transform (DRIFT) spectra. We expect higher and more variable C=C (aromatic) relative to C=O in POM than in MAOM (Fig. 1e Decoupled hypothesis). Most aromatic C=C is derived from plants while C=O is often contributed by microbes (Christensen, 2001; Nocentini et al., 2010; Miltner et al., 2012; Heckman et al., 2013; Hall et al., 2018). We also expect higher and more variable C-H (aliphatic) relative to C=O in POM than in MAOM (Fig. 1e Decoupled hypothesis). Higher C-H (aliphatic) in POM has been related to a major contribution of plants to POM (Demyan et al., 2012; Laudicina et al., 2015). Finally, we expect that MAOM should have consistently higher  $\delta^{13}$ C values than POM (Fig. 1f Decoupled hypothesis) as a result of  $\bar{^{13}}\text{C-enrichment}$  in microbial biomass as compared to plants and whole SOM (Werth and Kuzyakov, 2010; Klink et al., 2022). Similarly, MAOM should have higher  $\delta^{15}N$  than POM (Fig. 1f Decoupled hypothesis), due to <sup>15</sup>N-enriched microbial biomass as well as fractionating losses during repeated cycling of N in SOM (Craine et al., 2015; Klink et al., 2022).

Nevertheless, microbial necromass is not the only contributor to MAOM. Soluble constituents of plant litter have long been known to preferentially sorb to minerals (Kalbitz and Kaiser, 2008; Kramer et al., 2012). Substantial and even major contributions of plant-derived C to

MAOM have been shown (Fig. 1b Coupled hypothesis; Coward et al., 2018; Córdova et al., 2018; Huang et al., 2019; Angst et al., 2021). In these cases, we expect that POM and MAOM should have relatively coupled C/N, similar C functional groups measured by DRIFT, and similar  $\delta^{13}$ C and  $\delta^{15}$ N values (Fig. 1c, d, 1e, and 1f Coupled hypotheses). Note that the "decoupled" and "coupled" hypotheses are not mutually exclusive; rather, they represent two end members of a continuum. Given the divergent implications of coupled vs decoupled POM and MAOM for how we understand and model soil carbon cycling, we sought to evaluate these differing hypotheses.

Moreover, if the degree of coupling/decoupling varies, it is important to uncover which environmental factors predict these differences among diverse soils. Soil pH, silt and clay particles containing reactive minerals, temperature, and precipitation all had disparate relationships with SOC mass in POM and MAOM fractions (Song et al., 2012; Benbi et al., 2014; Haddix et al., 2020; Lugato et al., 2021). Forests had generally higher C/N in POM relative to grasslands and C/N in MAOM was negatively related to silt + clay and pH in a study across Europe (Cotrufo et al., 2019). We thus expect that the difference in C/N between POM and MAOM would increase with increasing silt + clay and pH and be larger in forests compared with other ecosystems. Compared with SOC mass and C/N, there is little research on how these environmental conditions, especially geochemical factors, would affect differences in isotopic and chemical composition between POM and MAOM. Reactive minerals and/or metals including aluminum (Al), iron (Fe), and calcium (Ca) play important roles in SOC protection (Torn et al., 1997; Rasmussen et al., 2018; Rowley et al., 2018; Yu et al., 2021). Thus, we expect that increasing reactive minerals and metals could increase the C content in MAOM relative to POM. As organic matter decomposes, the remaining C usually becomes more oxidized with lower C-H (aliphatic)/C=O (Ryals et al., 2014) and more likely to bind with minerals. Therefore, we predict that increasing reactive minerals would correspond to greater coupling of C-H (aliphatic)/C=O between POM and MAOM. We also expect that increasing reactive minerals and metals could lead to greater adsorption of aromatic C=C from soluble constituents of plant litter (Kalbitz and Kaiser, 2008; Kramer et al., 2012), increasing C=C (aromatic)/C=O in MAOM and greater coupling of C=C (aromatic)/C=O between POM and MAOM.

Here, we address where and why POM and MAOM differ among diverse soils, using replicate samples at 0-15 and 15-30 cm depths from 20 terrestrial sites in the National Ecological Observatory Network (NEON). These sites spanned diverse ecosystems, climatic zones (tundra to tropics), and soil orders across North America (Table S1). We compared C quantity and composition between the two fractions on a per-sample basis. We investigated relative importance of soil geochemistry, climate, and ecosystem type for explaining differences between the two fractions by linear mixed model (LMM) and random forest model (RFM). We assessed the capacity of POM and MAOM traits to predict cumulative SOC decomposition in laboratory incubations using partial least squares regression (PLSR), principal component analysis (PCA), and LMM. Leveraging the large-scale environmental gradient afforded by NEON sites, we ask: 1) where do POM and MAOM converge vs diverge in their C quantity and composition across these greatly contrasting soils? 2) do POM and MAOM have similar relationships with SOC decomposition? 3) can soil geochemistry, climate, and ecosystem type individually or jointly predict differences between the fractions?

# 2. Materials and methods

# 2.1. Site selection and soil sampling

All samples were collected from sites included in the NEON, a U.S. based, continental-scale ecological monitoring network that provides open data, samples, and research infrastructure to reveal how ecosystems are responding to environmental change (Keller et al., 2008). We

partnered with NEON to collect soil samples from 20 NEON terrestrial sites, denoted by their NEON acronyms as follows: BONA, CPER, DSNY, GRSM, HARV, KONZ, LENO, NIWO, ONAQ, OSBS, PUUM, SJER, SRER, SCBI, TALL, TOOL, UNDE, WREF, WOOD, YELL (Fig. S1). These sites span wide edaphic, climatic, and ecosystem gradients, from the tundra to the tropics (Table S1). These soils included 9 out of the 12 soil orders (no Histosols, Oxisols, or Vertisols) in the United States Department of Agriculture (USDA) soil classification system. The sites had mean annual temperature (MAT) of -9–22 °C, mean annual precipitation (MAP) of 262–2657 mm, and included diverse ecosystem types (forest, wetland, grassland, and shrubland).

Soils at each site were sampled by NEON staff in 2019. Most were sampled in April and May, and the colder sites were sampled in July/ August after thaw. Mineral soil samples were collected at two depths (0-15 cm and 15-30 cm following removal of any O horizon) around the perimeter of one 40 × 40-m "distributed base plot" which was selected to represent the dominant upland vegetation type and soil type of that site, whenever possible, in accordance with site access constraints. These two depths roughly correspond to A and B/E horizons, respectively. Despite different depths of A horizon across sites, 15 cm is the average bottom depth of A horizon across ten NEON sites with data on natural soil horizons (Table S2). For this study we used four sampling locations per plot (one from each side of the  $40 \times 40$ -m plot, 4 m outside of the plot boundary). Soils at the KONZ site were collected only at 0-15 cm due to the shallow soil depth. Soils were shipped overnight on ice (~4 °C) to Iowa State University (ISU). Each sample was gently homogenized inside a plastic bag after any coarse roots and macrofauna were manually removed. The following year (2020), a grab-sample of surface litter was collected from the plot in each site and shipped to ISU for chemical analysis.

#### 2.2. Soil geochemical analysis

Field-moist soil subsamples were measured for pH in 1:1 slurries of soil and deionized water. Air-dried subsamples were extracted with acid ammonium oxalate in the dark at pH 3 to measure organo-metal complexes and poorly crystalline phases of Al and Fe (denoted Alox and Feox), and with sodium citrate/dithionite to measure crystalline and poorly crystalline phases of Fe (Fe<sub>cd</sub>) as well as co-occurring Mn (Mn<sub>cd</sub>) and Ca (Cacd) (Loeppert and Inskeep, 1996). Metals were analyzed via inductively coupled plasma optical emission spectrometry (PerkinElmer Optima 5300 DV, Waltham, MA). The difference between Fe<sub>cd</sub> and Fe<sub>ox</sub> represents crystalline phases (Fe<sub>cd-ox</sub>). We interpret Mn<sub>cd</sub> as including exchangeable Mn, organo-metal complexes, and poorly crystalline phases, as Mn dissolved by oxalate and citrate-dithionite were very similar (data not shown). We interpret Cacd as a measure of exchangeable Ca and Ca in organo-Fe associations (Hall and Huang, 2017). Field-moist subsamples were also extracted with hydrochloric acid (HCl) to measure dissolved and adsorbed Fe(II) as well as dissolved or organically-complexed Fe(III) and a reactive fraction of Fe(III) minerals (Hall and Silver, 2015). Concentrations of Fe(II) and Fe(III) were measured colorimetrically using a ferrozine assay (Huang and Hall, 2017) and summed as Fe<sub>HCl</sub>.

#### 2.3. SOM fractionation method and fraction chemical analysis

Soil fractionation methods are varied and contentious, and all known methods yield fractions composite in nature and turnover rates (von Lützow et al., 2007; Poeplau et al., 2018). It should be acknowledged that all POM/MAOM fractions are operationally defined, because different fractionation methods yield different combinations of material along a continuum of plant detritus to mineral-associated phases (Wagai et al., 2020), and because even at nanometer scale, organic matter may be protected by aggregation rather than by organo-mineral complexes (Chenu and Plante, 2006). Protocols with sonication and density separation more precisely isolate distinct organo-mineral fractions, yet it is

challenging to optimize a single method for diverse soils, given differences in required sonication energy input and solution density (Wagai et al., 2015, 2020). Here, we used a classic method where POM and MAOM fractions were determined by size following chemical dispersion of aggregates (Cambardella and Elliott, 1992; Cotrufo et al., 2019), for a total of 312 fractions (156 soils × 2 fractions). This method has been shown to isolate fractions similar in size, biogeochemical properties, and turnover rates to density fractionation (Cambardella and Elliott, 1992; Six et al., 2002; Poeplau et al., 2018). More importantly, size fractionation can be consistently applied to diverse soils and requires less workload than density fractionation (Cotrufo et al., 2019).

To conduct the size fractionation, 10 g of air-dried and sieved (<2 mm) soil was shaken in 50 mL of 0.5% sodium hexametaphosphate dispersing solution for 18 h. The dispersed soil solution was rinsed onto a 53-μm sieve and organic material passing through (<53 μm) was defined as MAOM and organic material in the fraction remaining on the sieve (53-2000 µm) was defined as POM. In many cases this coarse fraction is dominated by sand; we emphasize that POM was measured directly by its C concentration and SOC mass in POM was obtained by POM SOC concentration multiplying by POM mass proportion (corresponding to sand content; see Supplemental equation (1)). The fine fraction containing MAOM was further separated into silt (2-53 µm) and clay (<2 µm) according to the difference in their sedimentation time (Kettler et al., 2001). The fractions settling to the bottom and suspended in water after 4 h were collected as silt and clay, respectively. The fractions were oven-dried at 60 °C to constant mass and were finely ground with a mortar and pestle.

The POM and MAOM (combined silt and clay) fractions as well as dried and finely ground samples of original (non-fractionated) soils and surface litter were analyzed for SOC and N concentrations,  $\delta^{13}$ C, and δ<sup>15</sup>N by an elemental analyzer coupled with isotope ratio mass spectrometer (ThermoFinnigan Delta Plus XL, Waltham, MA) at ISU. All samples at two sites (ONAQ and WOOD) had pH > 7 and mean carbonate >4 mg C g<sup>-1</sup> soil (Huang and Hall, 2018). Fractions from the two sites were fumigated by HCl for 72 h to remove carbonate prior to SOC and  $\delta^{13}$ C analysis (Harris et al., 2001). Some samples from sites CPER, SRER, and YELL had circumneutral pH, and NEON acidifies these sites for routine analyses to account for possible carbonate interferences. Yet all of our samples from these sites had measured carbonate < 0.1 mg C  $g^{-1}$  soil, thus they were not acidified. SOC mass and proportion of total SOC in each fraction were calculated and missing values in POM samples were estimated when they were below detection limits (Supplemental Materials and Methods).

Chemical composition of POM and MAOM were analyzed via diffuse reflectance infrared Fourier transform spectroscopy (DRIFT), a method that provides information on the abundance of different chemical functional groups of organic matter and/or minerals (Parikh et al., 2014). Spectra were recorded on a Fourier transform infrared (FTIR) spectrophotometer (Bruker Tensor 37, Ettlingen, Germany) with a diffuse reflectance apparatus (Harrick Scientific Seagull, Ossining, NY). Based on preliminary analyses that compared multiple sample preparation methods, most samples were homogenized in a 1:2 ratio with spectroscopy-grade KBr using a mortar and pestle; several samples with high SOC concentrations were prepared in a 1:10 ratio because the signal was too high for certain functional groups. Using finely ground KBr as a background reference, DRIFT spectra were measured between 4000 and 400  $\mathrm{cm}^{-1}$  averaged over 32 scans at 4  $\mathrm{cm}^{-1}$  resolution and converted to absorbance via the Kubelka-Munk function. The spectra were truncated to 4000-500 cm<sup>-1</sup> and baseline corrected before being imported into R. We selected the following broad regions for chemical composition analysis: peaks spanning 2826–3000 cm<sup>-1</sup> were attributed to aliphatic C–H stretch, a broad peak spanning 1550–1760 cm<sup>-1</sup> was attributed to C=O stretch, and a shoulder peak spanning 1480-1550 cm<sup>-1</sup> was attributed to aromatic C=C stretch (Figs. S2 and S3; Parikh et al., 2014; Ryals et al., 2014; Hall et al., 2018). Peak areas of the three regions were calculated and baseline areas were subtracted using the "approxfun" and "integrate" functions in R. Two ratios were used to indicate chemical composition of POM and MAOM. Increases in aromatic C=C (1480–1550 cm<sup>-1</sup>) relative to C=O (1550–1760 cm<sup>-1</sup>) may reflect increased contributions of plant-derived aromatic lignin/phenol/charcoal relative to microbially altered compounds (Nocentini et al., 2010; Heckman et al., 2013; Hall et al., 2018). Decreases in aliphatic C-H (2826–3000 cm<sup>-1</sup>) relative to C=O (1550–1760 cm<sup>-1</sup>) may reflect increased microbial oxidization (Ryals et al., 2014; Fissore et al., 2017) and/or decreased plant contribution (Demyan et al., 2012; Laudicina et al., 2015). HCl fumigation tended to greatly diminish one or all of the three regions (see representative DRIFT spectra from ONAQ in Figs. S2 and S3); untreated fractions from two sites with carbonates (ONAQ and WOOD) were thus used for DRIFT analyses despite the fact that carbonate peaks sometimes overlapped with the 1480–1550 cm<sup>-1</sup> shoulder peak.

#### 2.4. Lab incubation experiments

To measure SOC decomposition rate, additional soil subsamples (1 g dry mass equivalent) were brought to field moisture capacity and incubated under oxic conditions in the dark at 23 °C for 571 d. Soil was kept in an open 50 mL centrifuge tube inside a glass jar (946 mL) sealed with a gas-tight aluminum lid with butyl septa for headspace gas purging and sampling. The jars were flushed with CO2-free air following periodic headspace sampling as described below. Soil moisture was monitored by recording the mass of each sample, and water was added (every month before 179 d and every other month thereafter due to less frequent sampling) to replenish vapor lost during headspace flushing. Headspace gas was initially measured at 4 d and 11 d, every other week for another 140 d, and then every four weeks after 179 d. The CO<sub>2</sub> concentrations and their  $\delta^{13}$ C values were measured by a tunable diode laser absorption spectrometer (TDLAS, TGA200A, Campbell Scientific, Logan, UT) immediately prior to flushing the headspace (Hall et al., 2017). Two SOC decomposition variables, remaining percentage of initial SOC mass and cumulative decomposed SOC mass over 18 months were used in subsequent statistical models.

#### 2.5. Statistical analysis

All statistical analyses and plotting were performed in R statistical software version 3.6.1 (R Core Team, 2019). The map data were downloaded using the "get\_stamenmap" function in the "ggmap" package (Kahle and Wickham, 2013). Paired-sample T-tests were used to examine if means of proportion of total SOC, SOC concentration, C/N,  $\delta^{13}$ C, C=C (aromatic)/C=O, C-H (aliphatic)/C=O,  $\delta^{15}$ N, and SOC mass were significantly different between POM and MAOM. Linear mixed models (LMM) were used to identify important predictors for differences in C quantity and composition between the two fractions. In these models, we used values measured in POM minus the values measured in MAOM for each response variable, as a quantitative measure of similarity/difference between POM and MAOM for each attribute. Note that the order of subtraction (POM minus MAOM, vs. MAOM minus POM) is arbitrary for our purposes. Twelve predictors potentially important for differences between POM and MAOM were selected: soil pH, silt + clay,  $Al_{ox}$ ,  $Fe_{ox}$ ,  $Fe_{cd-ox}$ ,  $Fe_{HCl}$ ,  $Mn_{cd}$ ,  $Ca_{cd}$ , MAT, MAP, categorical ecosystem type, and depth. Based on preliminary analysis, six ecosystem types defined from the National Land Cover Database and provided by NEON were binned into three broad types: deciduous/evergreen forest (hereafter forest), grassland-herbaceous/shrub-scrub/dwarf scrub (grassland/shrubland), woody wetlands (wetland). Homoscedasticity and normality assumptions were met by raw data based on graphical assessment. All variables were standardized to a mean of zero and a standard deviation of one to estimate importance of predictors with different units. All predictor variables were used as fixed effects and site was included as a random intercept to account for possible intra-site dependence in the LMMs. Adding sampling location as an additional random effect to account for correlations between 0–15 and 15–30 cm samples did not improve model performance. All predictors exhibited variance inflation factor values <3 and correlation coefficients <0.70 or >-0.70, implying that collinearity was acceptable. Some predictors were removed from final models through comparison of Akaike Information Criterion (AIC) values of nested models using stepwise backward selection. The relative contributions of fixed effects were determined by standardized regression coefficient estimates, and their significance was tested by the Wald chi-square test. LMM performance was evaluated by  $\rm R^2$  representing variance explained by the model and by only the fixed effects, respectively. The LMM analyses were conducted with the "lme4" package (Bates et al., 2015).

Random forest models (RFM) (Breiman 2001) were also implemented to explore possible nonlinear relationships among predictors and differences in C quantity and composition between the two fractions. Variables were not standardized for an easier interpretation of the RFM partial dependency plot, which shows the marginal effect of each predictor on the predicted response variable. RFM was applied with 1000 trees, with other options sticking to default parameters in the "randomForest" package (Liaw and Wiener, 2002). RFM performance was evaluated by R<sup>2</sup> and variable importance was assessed using increase of mean squared error (%IncMSE) when a given variable is randomly permuted; a larger increase in MSE illustrates greater importance of the permuted variable. Variable importance as indicated by Z-score was further examined in the "Boruta" package (Kursa and Rudnicki, 2010).

Partial least squares regressions (PLSR) were used to compare whether DRIFT spectra of POM and MAOM could similarly predict SOC decomposition. The following steps were performed separately for POM and MAOM spectra. After comparing varying spectral processing methods and regions as well as sample partition algorithms (Table S3), the 4000-1340 cm<sup>-1</sup> spectral region, which receives less interference from soil minerals (Parikh et al., 2014), was selected due to generally higher predictive powers than other regions. The absorbance of each wavelength was normalized by a maximum absorbance within 1550–1760 cm<sup>-1</sup>, a dominant feature of SOM. To enhance the separation of overlapping peaks, the first derivative of the normalized spectra was calculated: the number of data points over which the derivative was taken and the segment size over which the function was smoothed was set to 11 and 10, respectively. The Kennard-Stone algorithm based on Euclidean distance was applied to identify 110 of the 156 samples that best accounted for variability in the spectra. The 110 samples were included in a calibration set, leaving the remaining 46 samples in a validation set. By regressing the response variable (C decomposition) on the principal components of scores decomposed from predictors (spectra), a PLSR model was developed on the calibration set and was tested on the independent validation set. To avoid overfitting, the appropriate number of principal components (maximum = 10) was determined by minimizing root mean square error using full cross validation in the calibration set. The correlation coefficient between model-predicted and measured decomposition in the validation set was used to assess how well DRIFT spectra could predict SOC decomposition. The PLSR analyses were conducted with the "pls" package (Mevik et al., 2016).

Principal component analyses (PCA) were also used to examine if SOC decomposition was significantly associated with DRIFT spectra. The PCAs were based on the baseline-corrected 4000–500 cm $^{-1}$  spectra, so as to examine whether spectral regions influenced by minerals and SOM would both relate to SOC decomposition. No further preprocessing of the spectra was applied. The PCAs were conducted with the "vegan" package (Oksanen et al., 2019). The SOC decomposition variables were fitted to the PCAs using the "envfit" function in the "vegan" package. Insignificant variables (P > 0.05) assessed by backward selection using Monte Carlo permutation tests were removed from the analysis.

LMMs were also used to compare prediction of SOC decomposition by POM and MAOM variables, respectively. Five C quantity and composition predictors of either POM or MAOM were selected: SOC mass, C/N,  $\delta^{13}$ C, C–H (aliphatic)/C=O, and C=C (aromatic)/C=O. Data processing, model fitting, and evaluation were similar as above. Decomposed SOC mass was log 10 transformed to meet statistical assumptions.

#### 3. Results

#### 3.1. Differences in C quantity and composition between POM and MAOM

Most response variables significantly differed (P < 0.05, paired ttests) between POM and MAOM fractions (Fig. S4), except for SOC mass  $(0.3-247.2 \text{ mg g}^{-1} \text{ soil})$ , mean = 16.3 mg g<sup>-1</sup> soil). However, variables often overlapped between the two fractions (Fig. S4) and were frequently correlated and similar on a per-sample basis, i.e., close to 1:1 lines (Fig. 2). We used normal linear regressions here for a more straightforward interpretation of relationships between POM and MAOM metrics, because linear mixed models accounting for the random effect of site showed similar results (data not shown). Partly consistent with both Fig. 1d Decoupled and Coupled expectations, although the C/ N ratios in POM were generally higher and more variable (8–45, mean = 19) than those in MAOM (7-27, mean = 14), C/N ratios of POM and MAOM were generally coupled (r = 0.85; Fig. 2a). Surface litter C/N varied greatly across 18 sites (27-99) and forests generally had higher litter C/N (mean = 61) than grassland/shrubland and wetland (mean = 45; Table S4). The C/N of MAOM was >15 in 9 out of 60 grassland/ shrubland samples and in 43 out of 80 forest samples; the 43 samples came from six forest sites (Fig. S5a), five of which had MAP >1200 mm (Table S1). Partly consistent with both Fig. 1e Decoupled and Coupled expectations, although the C=C (aromatic)/C=O ratio was greater on average in POM (0.04–0.30, mean = 0.11) than in MAOM (0.04–0.12, mean = 0.08), POM and MAOM often had similar ratios (i.e., many samples from different ecosystem types clustered near the 1:1 line in Fig. 2b). Consistent with Fig. 1e Coupled expectation, the C-H (aliphatic)/C=O ratios in POM (0-0.34, mean = 0.09) were correlated with (r = 0.76) and were often similar to those in MAOM (0-0.44), mean = 0.10; Fig. 2c). Partly consistent with both Fig. 1f Decoupled and Coupled expectations,  $\delta^{13}C$  values in MAOM (-29.0 to -14.6%, mean = -24.5%) were generally higher than those in POM (-29.6 to -15.0%, mean = -25.8%; r = 0.82; Fig. 2d), yet they were often close to the 1:1 line. The  $\delta^{15} N$  values in MAOM (–1.5–20.6‰, mean = 7.5‰) were consistently higher than those in POM (-1.3-18.7%, mean = 4.5%; r = 0.72; Fig. 2e). Notably, soils from three grassland/shrubland sites (CPER, SRER, WOOD) had much higher  $\delta^{13}$ C in MAOM than in POM (mean difference = 5.1%; Fig. S5b). POM constituted 2%–96% (mean = 41%) of total SOC while MAOM constituted 4%–98% (mean = 59%) of total SOC (Fig. S4g). A majority (50 out of 60) of grassland/ shrubland soils stored more SOC in MAOM than in POM while nearly half (32 out of 80) of forest soils stored more SOC in POM than in MAOM, especially for the eight evergreen tropical forest soils from

Besides ecosystem type, soil depth also affected how POM and MAOM differed in C–H (aliphatic)/C=O,  $\delta^{13}$ C, and SOC mass, but not in C/N, C=C (aromatic)/C=O, and  $\delta^{15}$ N (Fig. S6). The C–H (aliphatic)/C=O ratios in MAOM were correlated (r=0.64) with those in POM in 0–15 cm samples; the ratios were even more strongly correlated (r=0.82) with and mostly higher than those in POM in 15–30 cm samples (Fig. S6c). The  $\delta^{13}$ C values in POM were more correlated (r=0.92) with those in MAOM in 0–15 cm than 15–30 cm samples (r=0.65; Fig. S6d). Few (14 out of 76) soils had more C in POM than in MAOM in 15–30 cm while nearly half (35 out of 80) of soils had more C in POM than in MAOM in 0–15 cm samples (Fig. S6f).

#### 3.2. Predictors for differences between POM and MAOM

Two statistical models, LMM and RFM, identified important soil

geochemical, climate, and vegetation predictors for differences between the two fractions. The LMM showed that silt + clay, Fe $_{\rm ox}$ , MAP, and depth significantly (P < 0.05) predicted POM proportion of total SOC minus MAOM proportion of total SOC (Table 1). Silt + clay was negatively while MAP was positively related to the difference. The RFM also showed that these two predictors had IncMSE  $>\!20\%$  and further revealed nonlinear relationships between the difference and predictors (Fig. 3). Silt + clay and ecosystem type were consistently related to POM C/N minus MAOM C/N in both models (Table 1 and Fig. 3). Silt + clay had a positive relationship with the difference. Forests had a larger difference in C/N between POM and MAOM than grassland/shrubland and wetland soils (Fig. 3). No variables significantly predicted POM  $\delta^{13}$ C minus MAOM  $\delta^{13}$ C in the LMM (Table 1).

Both models identified important geochemical predictors for the difference in C=C (aromatic)/C=O between POM and MAOM (Table 1 and Fig. 3). Silt + clay and Ca<sub>cd</sub> were negatively related to the difference in the LMM. In the RFM, the difference decreased with initial increases in Alox (0.2–1.0 mg g $^{-1}$  soil), Fe $_{\rm ox}$  (0.1–0.8 mg g $^{-1}$  soil), and Fe $_{\rm HCl}$  (0.1–0.5 mg g $^{-1}$  soil) but remained constant at higher concentrations of these elements. Ca $_{\rm cd}$  and depth predicted the difference in C–H (aliphatic)/C=O between POM and MAOM in both models, and Ca $_{\rm cd}$  had a positive relationship with the difference.

The fixed-effect predictors explained 54% of the variation in POM proportion of SOC minus MAOM proportion of SOC in the LMM (Table 1). When incorporating the random effect of site, the LMMs explained >70% of the variation in differences between POM and MAOM in proportion of total SOC,  $\delta^{13}$ C, and C=C (aromatic)/C=O. Predictors also explained >65% of the variation in these differences in the RFM, and approximately 50% of the variation in differences in C/N and C-H (aliphatic)/C=O.

#### 3.3. Relationships of SOC decomposition with POM and MAOM

The PLSR analyses showed that SOC decomposition could be well predicted by DRIFT spectra of both POM and MAOM (Tables 2 and S3). Selected POM spectra could effectively predict decomposed SOC mass (r=0.87) and remaining SOC percentage (r=0.73) for the validation soils (Table 2). Selected MAOM spectra could also effectively predict decomposed SOC mass (r=0.70) and remaining SOC percentage (r=0.80) for the validation soils. We further confirmed that SOC decomposition could often be well predicted by both POM and MAOM spectra (r>0.70 for decomposed SOC mass and >0.60 for remaining SOC percentage), using varying spectral processing methods and regions as well as sample partition algorithms (Table S3).

The PCA plots showed no clear separation of DRIFT spectra by ecosystem type but they did show significant associations between POM spectra and remaining SOC percentage (Fig. 4a) and between MAOM spectra and decomposed SOC mass (Fig. 4c). The first two principal components (PC1 and PC2) explained 74.7% and 58.8% of the variation in overall POM and MAOM spectra, respectively. Scores of PC1 from POM spectra were positively correlated with remaining SOC percentage (r = 0.20; Fig. 4a) and scores from MAOM spectra were negatively correlated with decomposed SOC mass (r = -0.27; Fig. 4c). For both POM and MAOM spectra, loadings of PC1 were mostly positive within 4000–500 cm<sup>-1</sup> and larger within regions influenced by mineral absorbance (e.g., 3800-3000 and 1200-500 cm<sup>-1</sup>) than from those mainly caused by SOM absorbance (e.g., 3000-2800 and 1760-1300 cm<sup>-1</sup>; Fig. 4b and d). Scores of PC2 had weaker relationships with SOC decomposition (r = 0.12 for remaining SOC percentage in POM in Fig. 4a and r = 0.04 for decomposed SOC mass in MAOM in Fig. 4c).

The LMM analyses showed that POM and MAOM variables were both significantly related to SOC decomposition (Table 3). Optimum models containing all potential POM predictors (except for  $\delta^{13}$ C) and all MAOM predictors (except for C–H (aliphatic)/C=O) could explain 67% and 41% of the variation in decomposed SOC mass, respectively. SOC mass in POM was most important in the model using POM predictors (POM

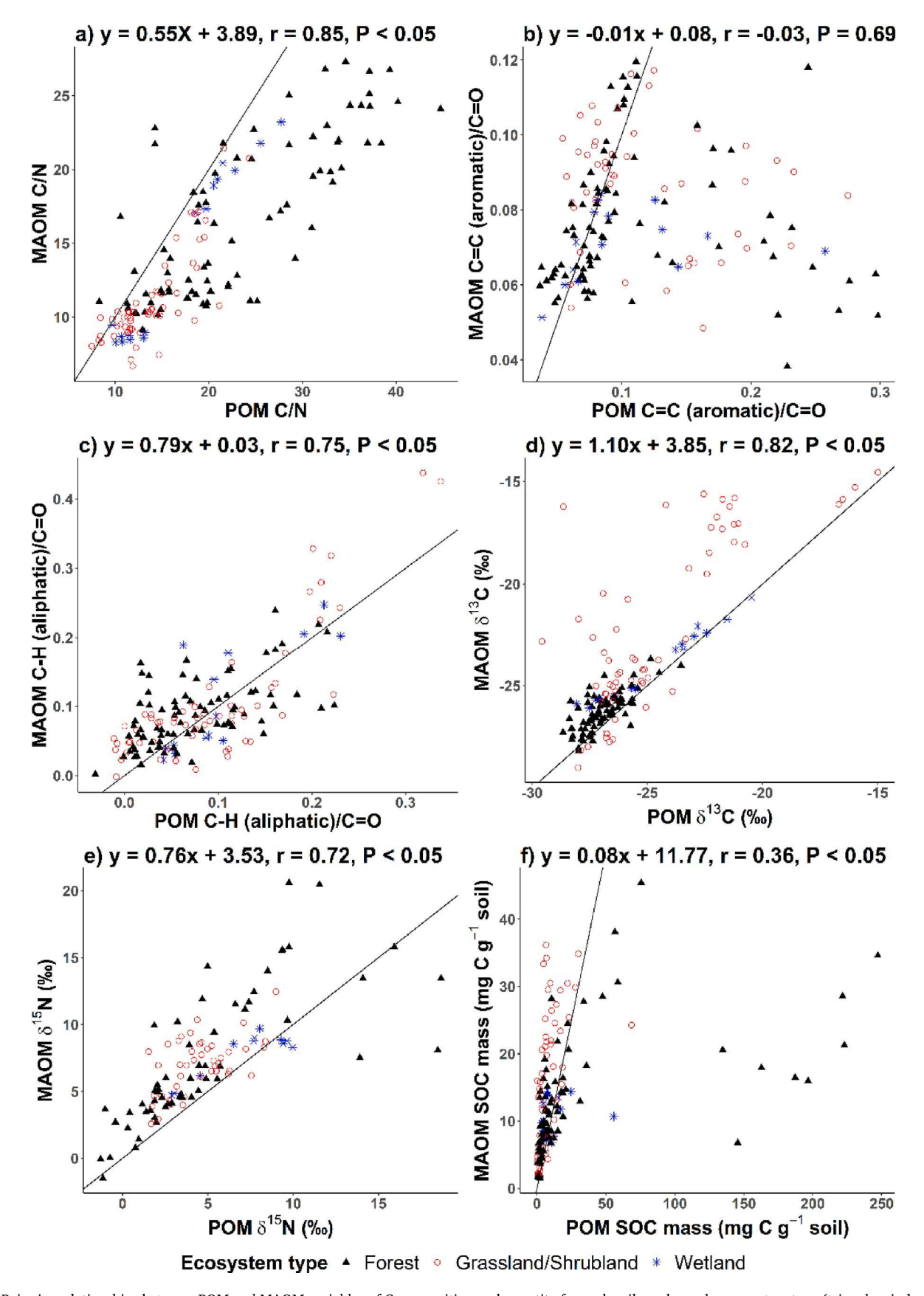


Fig. 2. Pairwise relationships between POM and MAOM variables of C composition and quantity for each soil, as shown by ecosystem type (triangle, circle, and star represent forest, grassland/shrubland, and wetland, respectively). Results of normal linear regressions and pairwise correlations are presented for a straightforward interpretation. The solid line represents a 1:1 relationship. C/N, C=C (aromatic)/C=O, C-H (aliphatic)/C=O,  $\delta^{13}$ C,  $\delta^{15}$ N, and SOC mass had 155, 142, 155, 156, 111, and 156 pairs of samples, respectively.

**Table 1**Statistical models predicting differences between POM and MAOM.

Predictors	Proportion of total SOC		C/N		$\delta^{13}$ C		C=C (aromatic)/C=O		C–H (aliphatic)/C=O	
	LMM	RFM								
$R^2$	$R_{fixed}^2 = 0.54$ $R_{model}^2 = 0.83$	$R^2 = 0.68$	$R_{fixed}^2 = 0.26$ $R_{model}^2 = 0.48$	$R^2 = 0.44$	$R_{fixed}^2 = 0.31$ $R_{model}^2 = 0.72$	$R^2 = 0.66$	$R_{fixed}^2 = 0.45$ $R_{model}^2 = 0.77$	$R^2 = 0.67$	$R_{fixed}^2 = 0.27$ $R_{model}^2 = 0.52$	$R^2 = 0.50$
Importance	Standardized coefficient	IncMSE %								
pН	-0.13	23.4	=	12.4	=	13.6	=	5.8	_	20.3
Silt + Clay	-0.55*	22.0	0.36*	19.3	0.11	15.7	-0.22*	16.0	0.15	15.8
Ca <sub>cd</sub>	0.14	23.5	_	25.7	_	12.6	-0.82*	6.5	0.32*	23.6
$Al_{ox}$	_	20.0	_	15.7	_	17.2	-0.08	23.9	_	16.5
Feox	0.15*	18.5	_	16.7	_	16.8	_	26.4	_	13.1
Fe <sub>cd-ox</sub>	_	16.7	-0.22	15.3	_	7.1	_	19.5	0.20	12.0
Fe <sub>HCl</sub>	_	13.3	_	9.8	_	13.4	_	24.8	0.10	18.6
$Mn_{cd}$	_	9.5	_	8.9	_	11.4	_	6.6	_	21.3
MAT	-0.22	19.5	_	14.9	-0.36	14.2	0.50*	15.3	_	19.5
MAP	0.42*	40.6	=	16.7	0.24	20.2	-0.19	15.0	_	16.5
Ecosystem type <sup>a</sup>	=	6.4	*	21.4	=	13.6	=	9.9	-	8.5
Depth	*	19.9	_	_	=	_	*	_	*	4.7

<sup>\*</sup> denotes P < 0.05 in the linear mixed model (LMM); — denotes retained in the LMM but P > 0.05.

model); SOC mass in MAOM was most important in the model using MAOM predictors (MAOM model). Optimum models containing all POM predictors (except for  $\delta^{13}\text{C})$  and all five MAOM predictors could explain 22% and 25% of the variation in remaining SOC percentage, respectively.

#### 4. Discussion

#### 4.1. Similarities and differences in composition between POM and MAOM

Despite the overall significant differences among measures of POM and MAOM composition, C/N,  $\delta^{13}$ C, and C-H (aliphatic)/C=O of POM and MAOM were strongly correlated and these metrics as well as C=C (aromatic)/C=O of POM and MAOM fell close to the 1:1 line in many samples (Fig. 2). These findings partially challenge expectations based on the MEMS hypothesis (Fig. 1b Decoupled), where composition of POM and MAOM are presumed to diverge during the transformation of plant residues into microbial necromass (Fig. 1c, d, 1e, and 1f Decoupled). The overall strong similarities between variables measured in POM and MAOM (Fig. 2, often corresponding to Fig. 1d, e, and 1f Coupled) are consistent with substantial or even dominant contributions of plant-derived OM to MAOM (Fig. 1b Coupled) for at least some soils in our dataset. Given the large differences in C/N between surface litter (27-99 across these NEON sites; Table S4) and microbes (typically 3-15; Cleveland and Liptzin, 2007; Strickland and Rousk, 2010), our observations of relatively low and constrained C/N values in MAOM support greater microbial contributions while higher and more variable C/N in POM reflect major contributions from plant litter (Fig. 2a, consistent with Fig. 1d Decoupled). However, these hypotheses do not explain the coupled C/N values of POM and MAOM observed for many samples (Fig. 2a, corresponding to Fig. 1d Coupled), which are instead consistent with a similar organic matter source to both fractions and a significant role of plant litter in MAOM (Fig. 1b Coupled). Furthermore, the C/N of MAOM was often >15 (Fig. 2a), inconsistent with the proposed range of MAOM C/N for soils with dominant microbial contributions to MAOM (8-13; Lavallee et al., 2020).

Metrics of isotopic and DRIFT-derived chemical composition also point to variable contributions of plant litter in MAOM (Fig. 1b Coupled). Partly consistent with both Fig. 1e decoupled and coupled hypotheses, while C=C (aromatic)/C=O ratio was larger in POM than

in MAOM for some soils, the ratio was also similar between POM and MAOM for many soils (Fig. 2b), pointing to likely contributions of plantderived C to MAOM. In these cases, dissolved organic matter from plant litter, e.g., carboxylated aromatics such as lignin polyphenols and charcoal, may have been selectively adsorbed to minerals and coprecipitated with metals (Kalbitz and Kaiser, 2008; Kögel-Knabner et al., 2008; Kramer et al., 2012; Hall et al., 2020) and provided the source of aromatic C=C in MAOM. Similar C-H (aliphatic)/C=O between POM and MAOM (Fig. 2c, corresponding to Fig. 1e Coupled) also suggest substantial contributions of plant-derived C to MAOM because higher C–H (aliphatic) has been related to more plant-derived C (Demyan et al., 2012; Laudicina et al., 2015). Frequent similarities in  $\delta^{13}$ C values between POM and MAOM (Fig. 2d, often corresponding to Fig. 1f Coupled) also likely reflect cases where MAOM had significant plant litter contributions. Because microbial biomass tends to have higher  $\delta^{13}$ C values than plant or soil C (Werth and Kuzyakov, 2010; Klink et al., 2022), we would expect higher  $\delta^{13} C$  in MAOM than in POM if microbial-derived Cis a major source of MAOM. Overall, the coupled and often overlapping elemental, isotopic, and chemical composition between POM and MAOM in soils from diverse environments indicate that microbial and plant residues contribute to both of these factions to varying extents (Córdova et al., 2018; Huang et al., 2019; Angst et al., 2021), highlighting that both plant- and microbial-derived C should be considered for MAOM.

Plant-derived C may especially contribute to MAOM in wet forests with MAP >1200 mm. Consistent with European studies (Cotrufo et al., 2019; Giannetta et al., 2019), the C/N of MAOM was generally <15 in grassland/shrubland sites but was >15 in five wet forest sites with MAP >1200 mm (Figs. 2a and S5a), suggesting a larger contribution of plant-derived C to MAOM in wet forests. The observations of MAOM C/N < 15 in grasslands can be attributed to fast microbial turnover of high quality litter under favorable pH conditions and thus a major proportion of microbial-derived C to MAOM (Angst et al., 2021). In contrast, frequently high lignin and charcoal concentrations in forested NEON sites (Hall et al., 2020), along with wet conditions favoring downward movement of soluble aromatic compounds, could result in larger contributions of plant-derived products to MAOM and greater C/N of MAOM in wet forests.

Soils from three grassland/shrubland sites (CPER, SRER, and WOOD) had much higher  $\delta^{13}\text{C}$  values in MAOM than in POM, especially for

<sup>-</sup> denotes predictors deemed unimportant and removed from the model by AIC using stepwise backward selection in the LMM or by the boruta approach in the RFM. % IncMSE in the RFM shows the increase of the mean squared error when a given predictor is randomly permuted. The larger the value, the more important the predictor.

<sup>&</sup>lt;sup>a</sup> Ecosystem type is a categorical variable, so a regression coefficient is not shown.

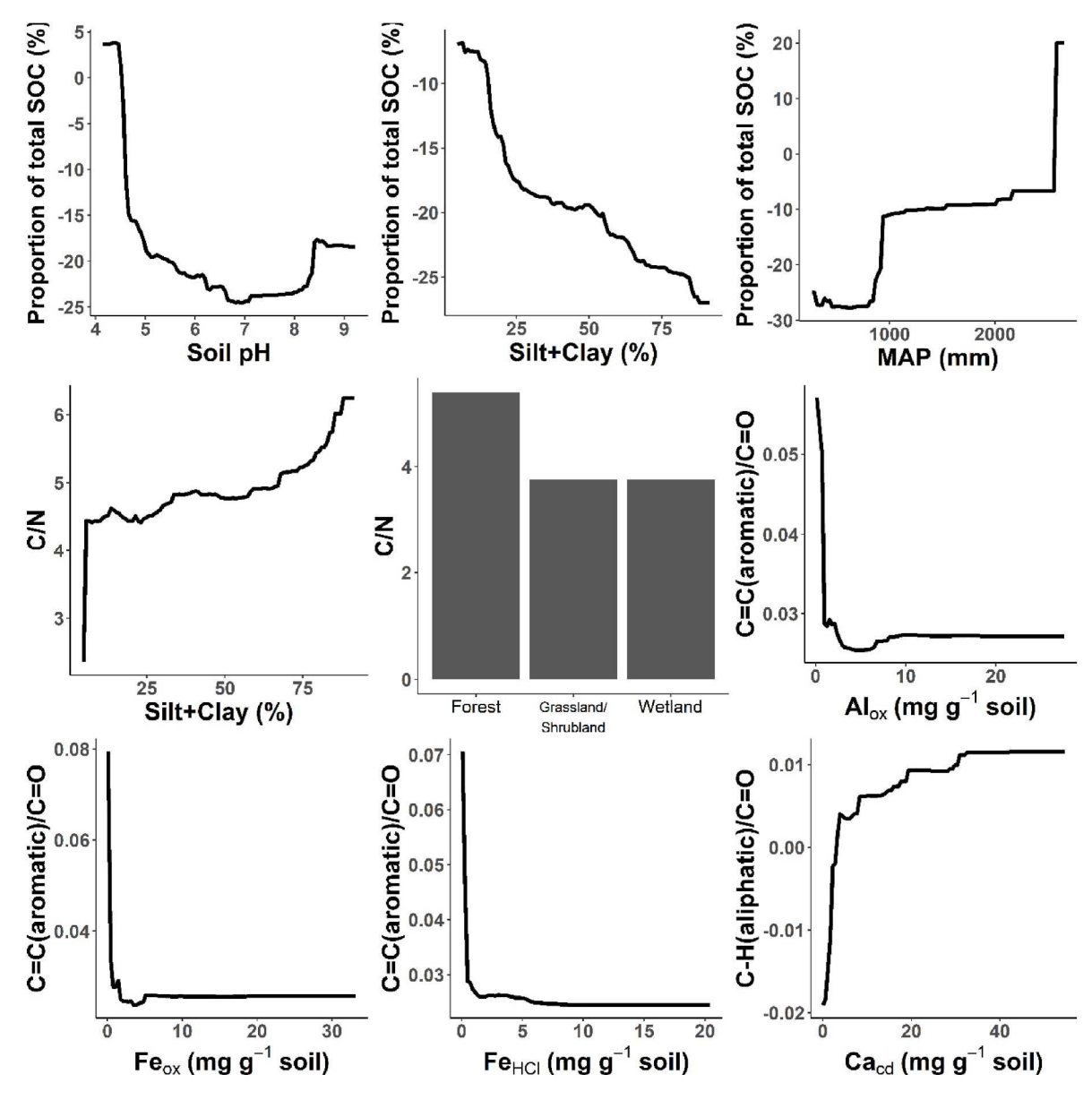


Fig. 3. Partial dependence plots of the random forest model (RFM) showing selected marginal effects of predictors on the predicted differences between POM and MAOM, i.e., POM variable - MAOM variable.

 $\begin{tabular}{ll} \textbf{Table 2} \\ \textbf{Model performance based on partial least squares regression (PLSR) to predict} \\ \textbf{SOC decomposition using POM and MAOM DRIFT spectra (4000–1340 cm$^{-1}$)}. \\ \end{tabular}$ 

C decomposition	Dataset	POM	POM		MAOM	
		r	RMSEP	r	RMSEP	
Decomposed SOC (mg C g <sup>-1</sup> soil) Remaining SOC (% of initial C mass)	calibration validation calibration validation	0.56 0.87 0.65 0.73	4.6 5.5 13.9 14.5	0.54 0.70 0.46 0.80	6.8 4.7 18.6 10.1	

r, correlation coefficient; RMSEP, root mean square error of prediction.

15–30 cm (Fig. S5b). These differences (mean = 5.1‰) are much larger than typical differences between plant and microbial sources (usually <2.5‰; Werth and Kuzyakov, 2010). Ruling out the possibility of carbonate interference in MAOM in these sites, these differences could reflect variable contributions of  $C_3$  (mean  $\delta^{13}C = -27\%$ ) and  $C_4$  (mean  $\delta^{13}C = -13\%$ ; Werth and Kuzyakov, 2010) plants to POM vs. MAOM as a consequence of variation in plant composition and OM inputs, such as

niche partitioning observed among  $C_3$  and  $C_4$  species at fine spatial and temporal scales (e.g., Martin et al., 2014).

# 4.2. Predictors for differences in C quantity and composition between POM and MAOM

We found that differences in POM and MAOM characteristics across the diverse NEON soils could be predicted in part by climate, ecosystem, and soil physicochemical properties (Table 1 and Fig. 3). The strong negative effect of silt + clay concentration on POM proportion of SOC minus MAOM proportion of SOC indicates that relatively more C can be stored by MAOM in soils with more fine particles, consistent with the finding of Haddix et al. (2020). MAP increased C stored in POM but not in MAOM and was positively related to the difference in proportion of SOC between POM and MAOM. This finding is consistent with the report that increased precipitation significantly stimulated POM C in North China (Song et al., 2012) but inconsistent with findings that MAOM accumulation was related to increasing MAP in North America (Follett et al., 2015; Haddix et al., 2020). Increasing MAP might favor POM

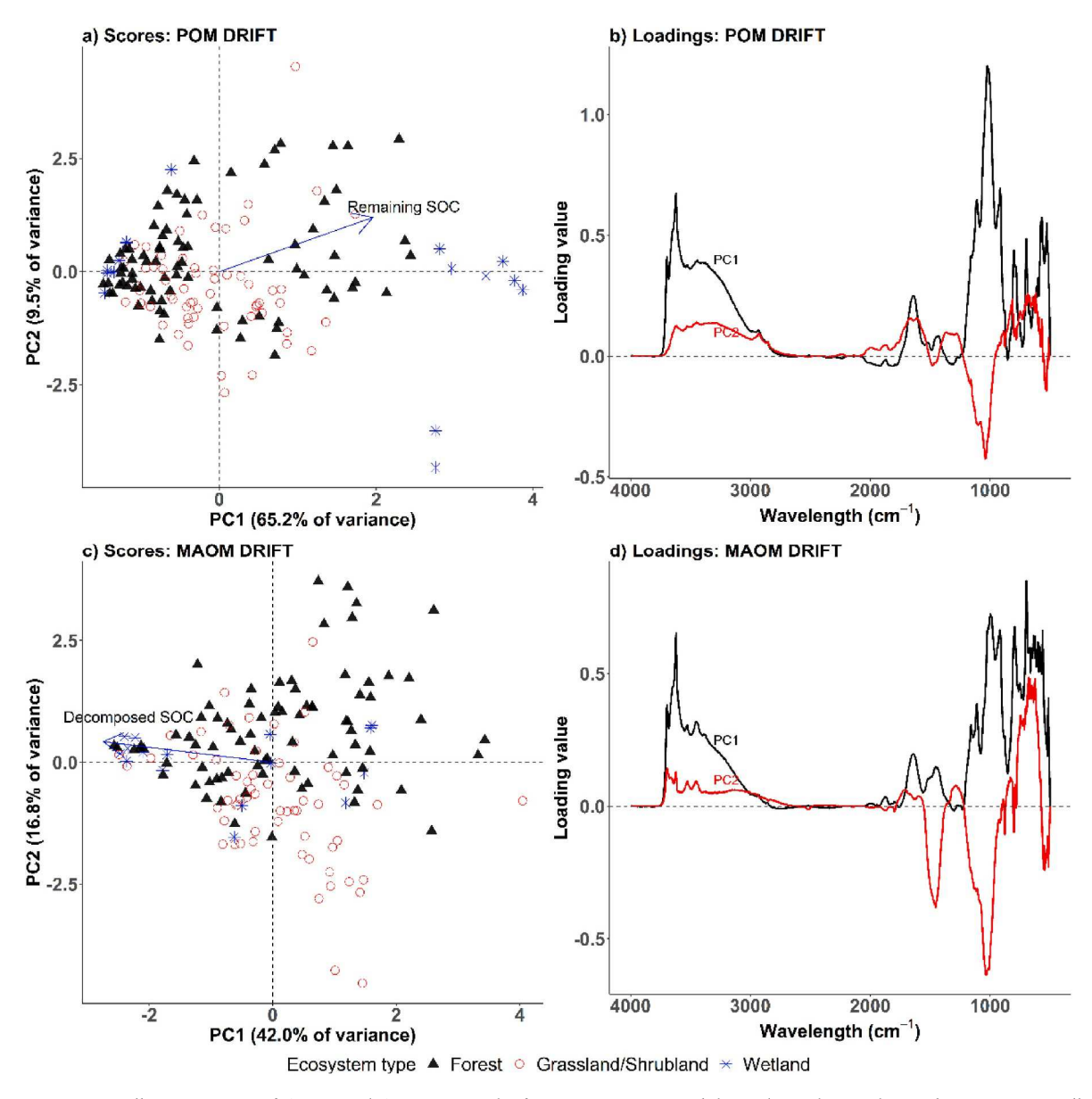


Fig. 4. Variations in overall DRIFT spectra of a) POM and c) MAOM samples from 20 NEON sites and their relationships with SOC decomposition as illustrated by score plots of principle component analysis (PCA). Vectors on score plots a) and c) indicate the direction of the increasing gradient for each variable, with the length of an arrow proportional to the correlation between ordination axes and an explanatory variable. Insignificant correlations (P > 0.05) were removed from the plots. The loading plots b) and d) show how strongly each wavelength influences PC1 (black) and PC2 (red) in POM and MAOM, respectively. The larger the absolute loading value, the stronger the influence. Triangle, circle, and star represent forest, grassland/shrubland, and wetland, respectively. (For interpretation of the references to color in this figure legend, the reader is referred to the Web version of this article.)

accumulation through increases in plant C input to POM, even if decomposition also increased (Song et al., 2012). Soil pH had a negative effect on POM proportion of SOC minus MAOM proportion of SOC and this effect was more pronounced below pH 5 in the RFM, suggesting that inhibited microbial decomposition caused by low pH favors POM accrual (Lugato et al., 2021). Although ecosystem type was less important for predicting POM proportion of SOC minus MAOM proportion of SOC, most grassland/shrubland soils stored more SOC in MAOM than in POM while nearly half of forest soils stored more SOC in POM than in MAOM (Fig. 2f). Similarly, SOM in European ectomycorrhizal forests was dominated by POM while grasslands and arbuscular mycorrhizal forests were dominated by MAOM (Cotrufo et al., 2019). Overall, our results indicate that POM accrual is favored in acidic and wet conditions while MAOM accrual is favored by fine particles, partly consistent with Christensen et al. (2001).

Soil geochemical composition was also related to differences in C

composition between POM and MAOM (Table 1 and Fig. 3). Consistent with a study using soils in European forests and grasslands (Cotrufo et al., 2019), forests generally had higher POM C/N relative to grassland/shrubland and wetland, owing to higher litter C/N in forests than grassland/shrubland and wetland (Table S4). The positive relationship between POM C/N minus MAOM C/N and silt + clay are consistent with the finding of a lower MAOM C/N with increasing silt + clay across Europe (Cotrufo et al., 2019), reflecting that more fine particles favor the accumulation of microbial products in MAOM. The difference in C=C (aromatic)/C=O decreased sharply with initial increases of reactive minerals or metals (Alox, Feox, FeHCl) but remained constant at higher levels (Fig. 3). These patterns may indicate that soluble constituents of plant litter are easily adsorbed but sorption sites are quickly saturated (Baldock and Skjemstad, 2000). We also observed a positive relationship between the difference in C–H (aliphatic)/C $\equiv$ O and Ca<sub>cd</sub>, mainly attributed to lower MAOM C-H (aliphatic)/C=O as Cacd

**Table 3**Optimal predictors of SOC decomposition based on linear mixed model (LMM) using POM and MAOM variables of C quantity and composition.

Predictor of POM or MAOM	Decomposed S soil)	OC (mg C g <sup>-1</sup>	Remaining SOC (% of initial C mass)		
	POM	MAOM	POM	MAOM	
	$R_{fixed}^2 = 0.67$ $R_{model}^2 = 0.80$	$R_{fixed}^2 = 0.41$ $R_{model}^2 =$ $0.76$	$R_{fixed}^2 = 0.22$ $R_{model}^2 =$ $0.62$	$R_{\rm fixed}^2 = 0.25$ $R_{\rm model}^2 = 0.59$	
SOC mass (mg C g <sup>-1</sup> soil)	0.66*	0.54*	-0.09	-0.24*	
C/N	-0.07	-0.14	-0.29*	-0.29*	
$\delta^{13}$ C	_	-0.18	_	0.21	
C–H (aliphatic)/ C=O	0.36*	=	-0.15	0.10	
C=C (aromatic)/ C=O	-0.08	0.15*	0.20*	-0.16	

 $<sup>^{\</sup>ast}$  denotes P < 0.05; numbers are regression coefficients of standardized variables.

increased. Exchangeable Ca appears to play an important role in SOC protection by bridging negatively charged sites in SOM and clay minerals (Rowley et al., 2018; Yu et al., 2021). Thus, increasing Ca<sub>cd</sub> would increase C content in MAOM, which usually becomes more oxidized and more likely to interact with minerals as organic matter decomposes. Soil depth also impacted the difference in C–H (aliphatic)/C—O. Despite the finding that the ratio was generally similar between POM and MAOM, MAOM seemed to be less oxidized than POM as indicated by higher C–H (aliphatic)/C—O ratios in MAOM in 15–30 cm of many soils (Fig. S6). Our findings reveal that soil geochemical composition can partly explain differences in elemental and chemical composition between POM and MAOM.

#### 4.3. MAOM was as good a predictor as POM for SOC decomposition

Multiple statistical analyses suggested that C quantity and composition of MAOM was similarly effective in predicting SOC decomposition as those of POM (Fig. 4; Tables 2 and 3). The PCA showed that SOC decomposition was more closely related to DRIFT spectra influenced by mineral composition than by those corresponding to SOM composition, as indicated by larger loadings of PC1 within the former vs. the latter spectral regions (Fig. 4b and d). However, the PLSR analyses showed that the DRIFT regions receiving less mineral absorbance well predicted SOC decomposition (Table 2). Thus, for both POM and MAOM, mineraland OM-influenced regions could both effectively predict SOC decomposition. In addition to overall DRIFT spectra, the LMM analyses also showed that POM and MAOM shared similar individual predictors for total SOC decomposition: SOC mass for decomposed SOC and C/N and C=C (aromatic)/C=O for remaining SOC (Table 3). Altogether, the findings suggest that attributes of POM and MAOM both effectively predicted SOC decomposition and these fractions also had similar predictors, probably because attributes of POM and MAOM were biogeochemically coupled (Fig. 2) and/or a large pool size of MAOM could compensate for its lower decomposition rate relative to POM (Christensen, 1987; Hall et al., 2015). Overall, our findings are consistent with the coupled evidence that both POM and MAOM were closely related to short-term SOC decomposition (Fig. 1a Coupled; Elliott, 1986; Christensen, 1987; Alvarez and Alvarez, 2000; Arevalo et al., 2012; Hall et al., 2015).

#### 4.4. Constraining effects of source mixing on MAOM interpretation

SOM fractionation methods based on size vs. density have different

caveats for interpretation. The <53  $\mu m$  fraction defined as MAOM in size fractionation protocols (Cambardella and Elliott, 1992; Cotrufo et al., 2019) also contains dissolved organic matter (DOM), fine particulate organic matter (POM <53  $\mu m$ ), and pyrogenic C, but previous literature along with a sensitivity analysis demonstrate that these contributions would not greatly affect our interpretations. First, contributions of DOM to our operational MAOM fraction are likely to be negligible. DOM usually makes up < 2% of total SOM and at least some DOM is actually derived from MAOM (von Lützow et al., 2007). Second, sensitivity analyses based on our data (Supplemental Discussion) indicate that mixing of a small proportion of fine POM with MAOM would not lead to different interpretations of our results. Third, much of the pyrogenic C in size-based MAOM fractions may actually be bound to minerals. Pyrogenic C occurs not only as particulate matter, but also interacts with minerals in clay-size (<2 μm) fractions (Brodowski et al., 2005; Cusack et al., 2012). In some long-term agricultural research stations in the U.S., dense fractions contained much more pyrogenic C than light fraction (Lavallee et al., 2019). Thus, we argue that any contributions of DOM, fine POM, and/or particulate pyrogenic C to our sized-based MAOM fractions would not substantially alter our conclusions.

#### 5. Conclusions

To conclude, this continental-scale study suggests that elemental, isotopic, and chemical composition of POM and MAOM were coupled and often overlapped across diverse soils. These data indicate that plant constituents were likely an important source of MAOM in many ecosystems, particularly in wet forests, suggesting that the MEMS hypothesis may not apply universally and should be considered along with other mechanisms of MAOM accrual. POM and MAOM had similar predictive performances for SOC decomposition, emphasizing that the importance of MAOM as a source of short-term SOC mineralization should not be overlooked. Soil geochemical composition could explain some of the observed differences between POM and MAOM, providing a path to predict differences in SOM fractions among diverse soils.

#### Research data for this article

The data on this study is available from the Environmental Data Initiative Data Portal: https://doi.org/10.6073/pasta/7fee15c1bed1aa 4b4c2aa397541cc83a.

# Declaration of competing interest

The authors declare that they have no known competing financial interests or personal relationships that could have appeared to influence the work reported in this paper.

# Acknowledgements

We are grateful to the NEON staff who facilitated this enormous sampling effort. This research was supported in part by NSF grant 1802745. The National Ecological Observatory Network is a program sponsored by the National Science Foundation and operated under cooperative agreement by Battelle. Data collected/used in this research were obtained through the NEON Assignable Assets program.

# Appendix A. Supplementary data

Supplementary data to this article can be found online at  $\frac{\text{https:}}{\text{doi.}}$  org/10.1016/j.soilbio.2022.108756.

denotes predictors removed from the model after deemed unimportant by AIC using stepwise backward selection.

#### References

- Alvarez, R., Alvarez, C.R., 2000. Soil organic matter pools and their associations with carbon mineralization kinetics. Soil Science Society of America Journal 64, 184–189. https://doi.org/10.2136/sssaj2000.641184x.
- Angst, G., Mueller, C.W., Prater, I., Angst, S., Frouz, J., Jílková, V., Peterse, F., Nierop, K. G.J., 2019. Earthworms act as biochemical reactors to convert labile plant compounds into stabilized soil microbial necromass. Communications Biology 2, 1–7. https://doi.org/10.1038/s42003-019-0684-z.
- Angst, G., Mueller, K.E., Nierop, K.G.J., Simpson, M.J., 2021. Plant- or microbial-derived? A review on the molecular composition of stabilized soil organic matter. Soil Biology and Biochemistry 156, 108189. https://doi.org/10.1016/j.soilbio.2021.108189.
- Arevalo, C., Chang, S., Bhatti, J. s, Sidders, D., 2012. Mineralization potential and temperature sensitivity of soil organic carbon under different land uses in the Parkland region of Alberta, Canada. Soil Science Society of America Journal 76, 241–251. https://doi.org/10.2136/sssaj2011.0126.
- Baldock, J.A., Skjemstad, J.O., 2000. Role of the soil matrix and minerals in protecting natural organic materials against biological attack. Organic Geochemistry 31, 697–710. https://doi.org/10.1016/S0146-6380(00)00049-8.
- Bates, D., Maechler, M., Bolker, B., Walker, S., 2015. Fitting linear mixed-effects models using lme4. Journal of Statistical Software 67, 1–48. https://doi.org/10.18637/jss. v067.i01.
- Benbi, D., Boparai, A., Brar, K., 2014. Decomposition of particulate organic matter is more sensitive to temperature than the mineral associated organic matter. Soil Biology and Biochemistry 70, 183–192. https://doi.org/10.1016/j. soilbjo.2013.12.032.
- Breiman, L., 2001. Random forests. Machine Learning 45, 5–32. https://doi.org/ 10.1023/A:1010933404324.
- Brodowski, S., Amelung, W., Haumaier, L., Abetz, C., Zech, W., 2005. Morphological and chemical properties of black carbon in physical soil fractions as revealed by scanning electron microscopy and energy-dispersive X-ray spectroscopy. Geoderma 128, 116–129. https://doi.org/10.1016/j.geoderma.2004.12.019.
- Cambardella, C.A., Elliott, E.T., 1992. Particulate soil organic-matter changes across a grassland cultivation sequence. Soil Science Society of America Journal 56, 777–783. https://doi.org/10.2136/sssaj1992.03615995005600030017x.
- Chenu, C., Plante, A.F., 2006. Clay-sized organo-mineral complexes in a cultivation chronosequence: revisiting the concept of the 'primary organo-mineral complex. European Journal of Soil Science 57, 596–607. https://doi.org/10.1111/j.1365-2389.2006.00834.x.
- Christensen, B.T., 2001. Physical fractionation of soil and structural and functional complexity in organic matter turnover. European Journal of Soil Science 52, 345–353. https://doi.org/10.1046/j.1365-2389.2001.00417.x.
- Christensen, B.T., 1996. Matching measurable soil organic matter fractions with conceptual pools in simulation models of carbon turnover: revision of model structure. In: Powlson, D.S., Smith, P., Smith, J.U. (Eds.), Evaluation of Soil Organic Matter Models Using Existing Long-Term Datasets. Springer-Verlag, Berlin, pp. 141–159.
- Christensen, B.T., 1987. Decomposability of organic matter in particle size fractions from field soils with straw incorporation. Soil Biology and Biochemistry 19, 429–435. https://doi.org/10.1016/0038-0717(87)90034-4.
- Cleveland, C.C., Liptzin, D., 2007. C:N:P stoichiometry in soil: is there a "Redfield ratio" for the microbial biomass? Biogeochemistry 85, 235–252. https://doi.org/10.1007/s10533-007-9132-0
- Córdova, S.C., Olk, D.C., Dietzel, R.N., Mueller, K.E., Archontouilis, S.V., Castellano, M. J., 2018. Plant litter quality affects the accumulation rate, composition, and stability of mineral-associated soil organic matter. Soil Biology and Biochemistry 125, 115–124. https://doi.org/10.1016/j.soilbio.2018.07.010.
- Cotrufo, M.F., Ranalli, M.G., Haddix, M.L., Six, J., Lugato, E., 2019. Soil carbon storage informed by particulate and mineral-associated organic matter. Nature Geoscience 12, 989–994. https://doi.org/10.1038/s41561-019-0484-6.
- Cotrufo, M.F., Wallenstein, M.D., Boot, C.M., Denef, K., Paul, E., 2013. The Microbial Efficiency-Matrix Stabilization (MEMS) framework integrates plant litter decomposition with soil organic matter stabilization: do labile plant inputs form stable soil organic matter? Global Change Biology 19, 988–995. https://doi.org/10.1111/gcb.12113.
- Coward, E.K., Ohno, T., Plante, A.F., 2018. Adsorption and molecular fractionation of dissolved organic matter on iron-bearing mineral matrices of varying crystallinity. Environ. Sci. Technol. 52, 1036–1044. https://doi.org/10.1021/acs.est.7b04953.
- Craine, J.M., Brookshire, E.N.J., Cramer, M.D., Hasselquist, N.J., Koba, K., Marin-Spiotta, E., Wang, L., 2015. Ecological interpretations of nitrogen isotope ratios of terrestrial plants and soils. Plant and Soil 396, 1–26. https://doi.org/10.1007/s11104-015-2542-1.
- Cusack, D.F., Chadwick, O.A., Hockaday, W.C., Vitousek, P.M., 2012. Mineralogical controls on soil black carbon preservation. Global Biogeochemical Cycles 26, GB2019. https://doi.org/10.1029/2011GB004109.
- Cyle, K.T., Hill, N., Young, K., Jenkins, T., Hancock, D., Schroeder, P.A., Thompson, A., 2016. Substrate quality influences organic matter accumulation in the soil silt and clay fraction. Soil Biology and Biochemistry 103, 138–148. https://doi.org/ 10.1016/j.soilbio.2016.08.014.
- Demyan, M.S., Rasche, F., Schulz, E., Breulmann, M., Müller, T., Cadisch, G., 2012. Use of specific peaks obtained by diffuse reflectance Fourier transform mid-infrared spectroscopy to study the composition of organic matter in a Haplic Chernozen. European Journal of Soil Science 63, 189–199. https://doi.org/10.1111/j.1365-2389.2011.01420.x.

- Elliott, E.T., 1986. Aggregate structure and carbon, nitrogen, and phosphorus in native and cultivated soils. Soil Science Society of America Journal 50, 627–633. https://doi.org/10.2136/sssai1986.0361595005000030017x.
- Feng, W., Shi, Z., Jiang, J., Xia, J., Liang, J., Zhou, J., Luo, Y., 2016. Methodological uncertainty in estimating carbon turnover times of soil fractions. Soil Biology and Biochemistry 100, 118–124. https://doi.org/10.1016/j.soilbio.2016.06.003.
- Fissore, C., Dalzell, B.J., Berhe, A.A., Voegtle, M., Evans, M., Wu, A., 2017. Influence of topography on soil organic carbon dynamics in a Southern California grassland. Catena 149, 140–149. https://doi.org/10.1016/j.catena.2016.09.016.
- Follett, R.F., Stewart, C.E., Pruessner, E.G., Kimble (Retired), J.M., 2015. Great Plains climate and land-use effects on soil organic carbon. Soil Science Society of America Journal 79, 261–271. https://doi.org/10.2136/sssaj2014.07.0282.
- Giannetta, B., Plaza, C., Zaccone, C., Vischetti, C., Rovira, P., 2019. Ecosystem type effects on the stabilization of organic matter in soils: combining size fractionation with sequential chemical extractions. Geoderma 353, 423–434. https://doi.org/ 10.1016/j.geoderma.2019.07.009.
- Griepentrog, M., Bodé, S., Boeckx, P., Hagedorn, F., Heim, A., Schmidt, M.W.I., 2014. Nitrogen deposition promotes the production of new fungal residues but retards the decomposition of old residues in forest soil fractions. Global Change Biology 20, 327–340. https://doi.org/10.1111/gcb.12374.
- Haddix, M.L., Gregorich, E.G., Helgason, B.L., Janzen, H., Ellert, B.H., Francesca Cotrufo, M., 2020. Climate, carbon content, and soil texture control the independent formation and persistence of particulate and mineral-associated organic matter in soil. Geoderma 363, 114160. https://doi.org/10.1016/j.geoderma.2019.114160.
- Hall, S.J., Berhe, A.A., Thompson, A., 2018. Order from disorder: do soil organic matter composition and turnover co-vary with iron phase crystallinity? Biogeochemistry 140, 93–110. https://doi.org/10.1007/s10533-018-0476-4.
- Hall, S.J., Huang, W., 2017. Iron reduction: a mechanism for dynamic cycling of occluded cations in tropical forest soils? Biogeochemistry 136, 91–102. https://doi. org/10.1007/s10533-017-0383-0.
- Hall, S.J., Huang, W., Hammel, K.E., 2017. An optical method for carbon dioxide isotopes and mole fractions in small gas samples: tracing microbial respiration from soil, litter, and lignin. Rapid Communications in Mass Spectrometry 31, 1938–1946. https://doi.org/10.1002/rcm.7973.
- Hall, S.J., McNicol, G., Natake, T., Silver, W.L., 2015. Large fluxes and rapid turnover of mineral-associated carbon across topographic gradients in a humid tropical forest: insights from paired <sup>14</sup>C analysis. Biogeosciences 12, 2471–2487. https://doi.org/ 10.5194/bg-12-2471-2015.
- Hall, S.J., Silver, W.L., 2015. Reducing conditions, reactive metals, and their interactions can explain spatial patterns of surface soil carbon in a humid tropical forest. Biogeochemistry 125. 149–165. https://doi.org/10.1007/s10533-015-0120-5.
- Hall, S.J., Ye, C., Weintraub, S.R., Hockaday, W.C., 2020. Molecular trade-offs in soil organic carbon composition at continental scale. Nature Geoscience 13, 687–692. https://doi.org/10.1038/s41561-020-0634-x.
- Harris, D., Horwáth, W.R., Kessel, C. van, 2001. Acid fumigation of soils to remove carbonates prior to total organic carbon or CARBON-13 isotopic analysis. Soil Science Society of America Journal 65, 1853–1856. https://doi.org/10.2136/ csci2001.1853
- Heckman, K., Grandy, A.S., Gao, X., Keiluweit, M., Wickings, K., Carpenter, K., Chorover, J., Rasmussen, C., 2013. Sorptive fractionation of organic matter and formation of organo-hydroxy-aluminum complexes during litter biodegradation in the presence of gibbsite. Geochimica et Cosmochimica Acta 121, 667–683. https:// doi.org/10.1016/j.gca.2013.07.043.
- Heckman, K., Hicks Pries, C.E., Lawrence, C.R., Rasmussen, C., Crow, S.E., Hoyt, A.M., von Fromm, S.F., Shi, Z., Stoner, S., McGrath, C., Beem-Miller, J., Berhe, A.A., Blankinship, J.C., Keiluweit, M., Marín-Spiotta, E., Monroe, J.G., Plante, A.F., Schimel, J., Sierra, C.A., Thompson, A., Wagai, R., 2022. Beyond bulk: density fractions explain heterogeneity in global soil carbon abundance and persistence. Global Change Biology 28, 1178–1196. https://doi.org/10.1111/gcb.16023.
- Huang, W., Hall, S.J., 2018. Large impacts of small methane fluxes on carbon isotope values of soil respiration. Soil Biology and Biochemistry 124, 126–133. https://doi. org/10.1016/j.soilbio.2018.06.003.
- Huang, W., Hall, S.J., 2017. Optimized high-throughput methods for quantifying iron biogeochemical dynamics in soil. Geoderma 306, 67–72. https://doi.org/10.1016/j. geoderma.2017.07.013.
- Huang, W., Hammel, K.E., Hao, J., Thompson, A., Timokhin, V.I., Hall, S.J., 2019. Enrichment of lignin-derived carbon in mineral-associated soil organic matter. Environmental Science & Technology 53, 7522–7531. https://doi.org/10.1021/acs.est.9b01834.
- Kahle, D., Wickham, H., 2013. ggmap: spatial Visualization with ggplot 2. The R Journal 5, 144–161.
- Kalbitz, K., Kaiser, K., 2008. Contribution of dissolved organic matter to carbon storage in forest mineral soils. Journal of Plant Nutrition and Soil Science 171, 52–60. https://doi.org/10.1002/jpln.200700043.
- Keiluweit, M., Bougoure, J.J., Nico, P.S., Pett-Ridge, J., Weber, P.K., Kleber, M., 2015. Mineral protection of soil carbon counteracted by root exudates. Nature Climate Change 5, 588–595. https://doi.org/10.1038/nclimate2580.
- Keller, M., Schimel, D.S., Hargrove, W.W., Hoffman, F.M., 2008. A continental strategy for the national ecological observatory network. Frontiers in Ecology and the Environment 6, 282–284. https://doi.org/10.1890/1540-9295(2008)6[282: ACSFTN]2.0.CO;2.
- Kettler, T.A., Doran, J.W., Gilbert, T.L., 2001. Simplified method for soil particle-size determination to accompany soil-quality analyses. Soil Science Society of America Journal 65, 849–852. https://doi.org/10.2136/sssaj2001.653849x.
- Kleber, M., Eusterhues, K., Keiluweit, M., Mikutta, C., Mikutta, R., Nico, P.S., 2015. Chapter One - mineral–organic associations: formation, properties, and relevance in

- soil environments. In: Sparks, D.L. (Ed.), Advances in Agronomy. Academic Press, Cambridge, Massachusetts, pp. 1–140. https://doi.org/10.1016/bs.agron.2014.10.005.
- Klink, S., Keller, A.B., Wild, A.J., Baumert, V.L., Gube, M., Lehndorff, E., Meyer, N., Mueller, C.W., Phillips, R.P., Pausch, J., 2022. Stable isotopes reveal that fungal residues contribute more to mineral-associated organic matter pools than plant residues. Soil Biology and Biochemistry 168, 108634. https://doi.org/10.1016/j. soilbio.2022.108634.
- Kögel-Knabner, I., Guggenberger, G., Kleber, M., Kandeler, E., Kalbitz, K., Scheu, S., Eusterhues, K., Leinweber, P., 2008. Organo-mineral associations in temperate soils: integrating biology, mineralogy, and organic matter chemistry. Journal of Plant Nutrition and Soil Science 171, 61–82. https://doi.org/10.1002/jpln.200700048.
- Kramer, M.G., Sanderman, J., Chadwick, O.A., Chorover, J., Vitousek, P.M., 2012. Long-term carbon storage through retention of dissolved aromatic acids by reactive particles in soil. Global Change Biology 18, 2594–2605. https://doi.org/10.1111/j.1365-2486.2012.02681.x.
- Kursa, M.B., Rudnicki, W.R., 2010. Feature selection with the Boruta package. Journal of Statistical Software 36, 1–13. https://doi.org/10.18637/jss.v036.i11.
- Laudicina, V.A., Novara, A., Barbera, V., Egli, M., Badalucco, L., 2015. Long-term tillage and cropping system effects on chemical and biochemical characteristics of soil organic matter in a Mediterranean semiarid environment. Land Degradation & Development 26, 45–53. https://doi.org/10.1002/ldr.2293.
- Lavallee, J.M., Conant, R.T., Haddix, M.L., Follett, R.F., Bird, M.I., Paul, E.A., 2019. Selective preservation of pyrogenic carbon across soil organic matter fractions and its influence on calculations of carbon mean residence times. Geoderma 354, 113866. https://doi.org/10.1016/j.geoderma.2019.07.024.
- Lavallee, J.M., Conant, R.T., Paul, E.A., Cotrufo, M.F., 2018. Incorporation of shoot versus root-derived <sup>13</sup>C and <sup>15</sup>N into mineral-associated organic matter fractions: results of a soil slurry incubation with dual-labelled plant material. Biogeochemistry 137, 379–393. https://doi.org/10.1007/s10533-018-0428-z.
- Lavallee, J.M., Soong, J.L., Cotrufo, M.F., 2020. Conceptualizing soil organic matter into particulate and mineral-associated forms to address global change in the 21st century. Global Change Biology 26, 261–273. https://doi.org/10.1111/gcb.14859.
- Liang, C., Schimel, J.P., Jastrow, J.D., 2017. The importance of anabolism in microbial control over soil carbon storage. Nature Microbiology 2, 1–6. https://doi.org/ 10.1038/nmicrobiol.2017.105.
- Liaw, A., Wiener, M., 2002. Classification and regression by random forest. R News 2, 18–22.
- Loeppert, R.H., Inskeep, W.P., 1996. Iron. In: Sparks, D.L., Page, A.L., Helmke, P.A., Loeppert, R.H., Soltanpour, P.N., Tabatabai, M.A., Johnston, C.T., Sumner, M.E. (Eds.), Methods of Soil Analysis. John Wiley & Sons, Ltd, pp. 639–664. https://doi.org/10.2136/sssabookser5.3.c23.
- Lugato, E., Lavallee, J.M., Haddix, M.L., Panagos, P., Cotrufo, M.F., 2021. Different climate sensitivity of particulate and mineral-associated soil organic matter. Nature Geoscience 14, 295–300. https://doi.org/10.1038/s41561-021-00744-x.
  Martin, L.M., Polley, H.W., Daneshgar, P.P., Harris, M.A., Wilsey, B.J., 2014.
- Martin, L.M., Polley, H.W., Daneshgar, P.P., Harris, M.A., Wilsey, B.J., 2014. Biodiversity, photosynthetic mode, and ecosystem services differ between native and novel ecosystems. Oecologia 175, 687–697. https://doi.org/10.1007/s00442-014-2911-0.
- Mevik, B.-H., Wehrens, R., Liland, K.H., 2016. Pls: Partial Least Squares and Principal Component Regression. R Package Version 2.6-0.
- Miltner, A., Bombach, P., Schmidt-Brücken, B., Kästner, M., 2012. SOM genesis: microbial biomass as a significant source. Biogeochemistry 111, 41–55. https://doi. org/10.1007/s10533-011-9658-z.
- Nocentini, C., Certini, G., Knicker, H., Francioso, O., Rumpel, C., 2010. Nature and reactivity of charcoal produced and added to soil during wildfire are particle-size dependent. Organic Geochemistry 41, 682–689. https://doi.org/10.1016/j. orggeochem.2010.03.010.
- Oksanen, J., Blanchet, F.G., Friendly, M., Kindt, R., Legendre, P., McGlinn, D., Minchin, P.R., O'Hara, R.B., Simpson, G.L., Solymos, P., Stevens, M.H.H., Szoecs, E., Wagner, H., 2019. Vegan: Community Ecology Package. R Package Version 2.5-4.
- Parikh, S.J., Goyne, K.W., Margenot, A.J., Mukome, F.N.D., Calderón, F.J., 2014. Chapter One - soil chemical insights provided through vibrational spectroscopy. In: Sparks, D.L. (Ed.), Advances in Agronomy. Academic Press, Cambridge, Massachusetts, pp. 1–148. https://doi.org/10.1016/B978-0-12-800132-5.00001-8.
- Parton, W.J., Schimel, D.S., Cole, C.V., Ojima, D.S., 1987. Analysis of factors controlling soil organic matter levels in Great Plains grasslands. Soil Science Society of America

- Journal 51, 1173–1179. https://doi.org/10.2136/sssai1987.03615995005100050015x.
- Paul, E.A., 2016. The nature and dynamics of soil organic matter: plant inputs, microbial transformations, and organic matter stabilization. Soil Biology and Biochemistry 98, 109–126. https://doi.org/10.1016/j.soilbio.2016.04.001.
- Poeplau, C., Don, A., Six, J., Kaiser, M., Benbi, D., Chenu, C., Cotrufo, M.F., Derrien, D., Gioacchini, P., Grand, S., Gregorich, E., Griepentrog, M., Gunina, A., Haddix, M., Kuzyakov, Y., Kühnel, A., Macdonald, L.M., Soong, J., Trigalet, S., Vermeire, M.-L., Rovira, P., van Wesemael, B., Wiesmeier, M., Yeasmin, S., Yevdokimov, I., Nieder, R., 2018. Isolating organic carbon fractions with varying turnover rates in temperate agricultural soils a comprehensive method comparison. Soil Biology and Biochemistry 125, 10–26. https://doi.org/10.1016/j.soilbio.2018.06.025.
- R Core Team, 2019. R: A Language and Environment for Statistical Computing. R Foundation for Statistical Computing, Vienna, Austria.
- Rasmussen, C., Heckman, K., Wieder, W.R., Keiluweit, M., Lawrence, C.R., Berhe, A.A., Blankinship, J.C., Crow, S.E., Druhan, J.L., Hicks Pries, C.E., Marin-Spiotta, E., Plante, A.F., Schädel, C., Schimel, J.P., Sierra, C.A., Thompson, A., Wagai, R., 2018. Beyond clay: towards an improved set of variables for predicting soil organic matter content. Biogeochemistry 137, 297–306. https://doi.org/10.1007/s10533-018-0424-3
- Rowley, M.C., Grand, S., Verrecchia, É.P., 2018. Calcium-mediated stabilisation of soil organic carbon. Biogeochemistry 137, 27–49. https://doi.org/10.1007/s10533-017-0410-1
- Ryals, R., Berhe, A.A., Torn, M.S., Kaiser, M., Silver, W.L., 2014. Impacts of organic matter amendments on carbon and nitrogen dynamics in grassland soils. Soil Biology and Biochemistry 68, 52–61. https://doi.org/10.1016/j.soilbio.2013.09.011.
- Six, J., Conant, R.T., Paul, E.A., Paustian, K., 2002. Stabilization mechanisms of soil organic matter: implications for C-saturation of soils. Plant and Soil 241, 155–176. https://doi.org/10.1023/A:1016125726789.
- Smith, J.U., Smith, P., Monaghan, R., MacDonald, A.J., 2002. When is a measured soil organic matter fraction equivalent to a model pool? European Journal of Soil Science 53, 405–416. https://doi.org/10.1046/j.1365-2389.2002.00458.x.
- Song, B., Niu, S., Zhang, Z., Yang, H., Li, L., Wan, S., 2012. Light and heavy fractions of soil organic matter in response to climate warming and increased precipitation in a temperate steppe. PLoS One 7, e33217. https://doi.org/10.1371/journal. ppg 0032317.
- Strickland, M.S., Rousk, J., 2010. Considering fungal:bacterial dominance in soils methods, controls, and ecosystem implications. Soil Biology and Biochemistry 42, 1385–1395. https://doi.org/10.1016/j.soilbio.2010.05.007.
- Torn, M.S., Kleber, M., Zavaleta, E.S., Zhu, B., Field, C.B., Trumbore, S.E., 2013. A dual isotope approach to isolate soil carbon pools of different turnover times. Biogeosciences 10, 8067–8081. https://doi.org/10.5194/bg-10-8067-2013.
- Torn, M.S., Trumbore, S.E., Chadwick, O.A., Vitousek, P.M., Hendricks, D.M., 1997. Mineral control of soil organic carbon storage and turnover. Nature 389, 170–173. https://doi.org/10.1038/38260.
- von Lützow, M., Kögel-Knabner, I., Ekschmitt, K., Flessa, H., Guggenberger, G., Matzner, E., Marschner, B., 2007. SOM fractionation methods: relevance to functional pools and to stabilization mechanisms. Soil Biology and Biochemistry 39, 2183–2207. https://doi.org/10.1016/j.soilbio.2007.03.007.
- Wagai, R., Kajiura, M., Asano, M., 2020. Iron and aluminum association with microbially processed organic matter via meso-density aggregate formation across soils: organometallic glue hypothesis. SOIL 6, 597–627. https://doi.org/10.5194/soil-6-597-2020
- Wagai, R., Kajiura, M., Asano, M., Hiradate, S., 2015. Nature of soil organo-mineral assemblage examined by sequential density fractionation with and without sonication: is allophanic soil different? Geoderma 241–242, 295–305. https://doi. org/10.1016/j.geoderma.2014.11.028.Werth, M., Kuzyakov, Y., 2010. <sup>13</sup>C fractionation at the root–microorganisms–soil
- Werth, M., Kuzyakov, Y., 2010. <sup>13</sup>C fractionation at the root–microorganisms–soil interface: a review and outlook for partitioning studies. Soil Biology and Biochemistry 42, 1372–1384. https://doi.org/10.1016/j.soilbio.2010.04.009.
- Witzgall, K., Vidal, A., Schubert, D.I., Höschen, C., Schweizer, S.A., Buegger, F., Pouteau, V., Chenu, C., Mueller, C.W., 2021. Particulate organic matter as a functional soil component for persistent soil organic carbon. Nature Communications 12, 4115. https://doi.org/10.1038/s41467-021-24192-8.
- Yu, W., Weintraub, S.R., Hall, S.J., 2021. Climatic and geochemical controls on soil carbon at the continental scale: interactions and thresholds. Global Biogeochemical Cycles 35, e2020GB006781. https://doi.org/10.1029/2020GB006781.